JOURNAL OF GUIDANCE, CONTROL, AND DYNAMICS
Vol. 33, No. 1, January–February 2010

Effects of Canopy-Payload Relative Motion on Control of Autonomous Parafoils

Nathan J. Slegers*
University of Alabama in Huntsville, Huntsville, Alabama 35899

DOI: 10.2514/1.44564

An eight-degree-of-freedom model is developed that accurately models relative pitching and yawing motion of a payload with respect to a parafoil. Constraint forces and moments are found analytically rather than using artificial constraint stabilization. A turn rate controller common in precision placement algorithms is used to demonstrate that relative yawing motion of the payload can result in persistent oscillations of the system. A model neglecting relative payload yawing failed to predict the same oscillations. It is shown that persistent oscillations can be eliminated by reduction of feedback gains; however, resulting tracking performance is poor. A reduced-order linear model is shown to be able to adequately predict relative payload dynamics for the proposed turn rate controller on the full eight-degree-of-freedom system.

Nomenclature

A, B, C, P, Q, R	=	Lamb's coefficients for apparent mass
a	=	ratio of derivative and proportional gain in yaw controller
$\vec{a}_{B/I}, \vec{a}_{S/I}$	=	mass center accelerations of the parafoil and payload
b	=	canopy span
C_{DS}	=	payload drag coefficient
C_{ij}	=	coefficient relating the ith dimensionless aerodynamic coefficient to the jth state
$\bar{c}$	=	canopy main chord
$\mathbf{E}_i$	=	3×1 column vector with a one on the ith element and zeros everywhere else
$\vec{F}_A, \vec{M}_A$	=	parafoil aerodynamic force and moment vectors in the body reference frame
$\vec{F}_{\mathrm{AM}}, \vec{M}_{\mathrm{AM}}$	=	apparent mass force and moment vectors in the body reference frame
F_{CX}, F_{CY}, F_{CZ}	=	connection constraint force components
$\vec{F}_{WB}, \vec{F}_{WS}$	=	weight vector of parafoil and payload in their respective frame
$\vec{F}_S$	=	payload drag vector in the payload reference frame
$\vec{H}_{B/I}, \vec{H}_{S/I}$	=	parafoil and payload angular momentum expressed in their respective frames
$I_{\mathrm{AM}}, I_{\mathrm{AI}}$	=	apparent mass and inertia matrices
I_B, I_S	=	parafoil and payload Inertia matrices
$\vec{I}_B, \vec{J}_B, \vec{K}_B$	=	body frame unit vectors
$\mathbf{I}_{N\times N}$	=	$N \times N$ identity matrix
$\vec{I}_P, \vec{J}_P, \vec{K}_P$	=	canopy frame unit vectors
$\vec{I}_S, \vec{J}_S, \vec{K}_S$	=	payload frame unit vectors
K_{FF}, K	=	yaw control feed forward and proportional gain
M_{CX}, M_{CZ}	=	connection constraint moment components
m_B, m_S	=	mass of the parafoil and payload
m_I	=	included air mass of the parafoil canopy
$\tilde{p}, \tilde{q}, \tilde{r}$	=	angular velocity of the parafoil in the canopy frame
p_B, q_B, r_B	=	parafoil angular velocity components in the body reference frame
p_S, q_S, r_S	=	payload angular velocity components in the payload reference frame
$\vec{r}_{XY}$	=	position vector from a point X to a point Y
$S^B_{\omega_B}, S^P_{\omega_B}$	=	cross-product matrix of the parafoil angular velocity expressed in the body and canopy reference frames
$S^B_{r_{BP}}, S^B_{r_{BM}}$	=	cross-product matrix of the vectors from the parafoil system mass center to the canopy aerodynamic center and apparent mass center
$S^B_{r_{CB}}, S^B_{r_{CM}}$	=	cross-product matrix of the vector from the point C to parafoil mass center and apparent mass center, both expressed in the body frame
S_P, S_S	=	reference area of the parafoil canopy and payload
$S^S_{r_{CS}}$	=	cross-product matrix of the vector from the point C to payload mass center, expressed in the payload frame
$S^S_{\omega_S}$	=	cross-product matrix of the payload angular velocity expressed in the payload reference frames
T_{AP}, T_{BP}	=	transformation from aerodynamic to canopy frame and from body to canopy frame
T_{BS}	=	transformation from the body to payload frame
T_{IB}	=	transformation from inertial to body frame
$\tilde{u}, \tilde{v}, \tilde{w}$	=	velocity components of the canopy aerodynamic center in the canopy reference frame
u_C, v_C, w_C	=	velocity components of connection point C in the body reference frame
u_{SA}, v_{SA}, w_{SA}	=	aerodynamic velocities of the payload in the payload frame
V_A, V_S	=	total aerodynamic speed of the parafoil canopy and payload
$\vec{V}_{A/I}$	=	velocity vector of the wind in an inertial reference frame
x_C, y_C, z_C	=	inertial position components of point C
x_{CB}, y_{CB}, z_{CB}	=	distance vector components from the point C to parafoil mass center in the body frame
x_{CR}, y_{CR}, z_{CR}	=	distance vector components from the point C to canopy rotation point in the body frame

Presented as Paper 2929 at the 20th AIAA Aerodynamic Decelerator Systems Technology Conference and Seminar, Seattle, WA, 4–7 May 2009; received 24 March 2009; revision received 31 August 2009; accepted for publication 2 September 2009.

*Assistant Professor, Department of Mechanical and Aerospace Engineering. Member AIAA.

x_{CS}, y_{CS}, z_{CS} = distance vector components from the point C to payload mass center in the payload frame
x_{RP}, y_{RP}, z_{RP} = distance vector components from the canopy rotation point to canopy aerodynamic center in the canopy frame
α, β = canopy angle of attack and sideslip
Γ = canopy incidence angle
δ_a = asymmetric brake deflection as a percentage of maximum deflection, $\in [-1, 1]$
θ_S, ψ_S = Euler pitch and yaw angles of the payload
ϕ_B, θ_B, ψ_B = Euler roll, pitch, and yaw angles of the parafoil
ψ = total yaw of the payload ($\psi_S + \psi_B$)
$\mathbf{0_{A\times B}}$ = zero matrix with dimension $A \times B$

I. Introduction

GUIDED parafoils are providing improved capability in performing a diverse set of military and civilian missions, such as precision airdrop, reconnaissance, troop resupply, and response to humanitarian crises. Parafoils are unique flight vehicles well suited to theses tasks because they fly at low speed and impact the ground with low velocity while maintaining the ability to be released at large offsets from the desired target. Additional attractive features of guided parafoils are their compact size before deployment and light weight.

An important component of all autonomous parafoils is the guidance algorithm. Many different types of guidance algorithms have appeared in literature, including dynamic programming, real-time optimal trajectory generation, linear predictive control, nonlinear predictive control, and flocking to name just a few [1–6]. A commonality between all these guidance strategies is an assumed dynamic model used for generation of the guidance algorithms. The types of models used for guidance are often low fidelity and include kinematic models, reduced-order models, and linearized versions of high-fidelity models. However, whereas simple models are used for designing the algorithms, higher-fidelity models are often used to evaluate performance in simulation or on actual systems.

Many aspects of parafoil systems make them difficult to accurately model. For example, the canopy and suspension lines are flexible structures allowing the possibility of changing shapes and aerodynamics. In addition, the canopy has a small mass-to-volume ratio resulting in so-called apparent mass forces and moments [7]. Another complication is the payload and canopy interaction. The payload and canopy can be connected using many configurations that allow a range of motion from free rotation of the payload with respect to the parafoil to a rigid canopy-payload connection. In practical applications some of the previous parafoil and payload characteristics can be ignored resulting in a range of models with varying degrees of freedom (DOF). The first level of model complexity is the 3-DOF and 4-DOF model for a parafoil and payload discussed by Jann [8]. The 3-DOF model included the horizontal motion of the mass center and the heading, whereas the 4-DOF model added roll with the latter achieving a reasonable match with flight data. The next level of complexity is a 6-DOF model where the payload and parafoil are considered one rigid body. Slegers and Costello used a simple 6-DOF model, excluding apparent mass, for predictive control [3]. Barrows developed a more complete 6-DOF model by including an accurate representation of apparent mass, including the effect from spanwise camber [9]. Later Slegers et al. developed a similar 6-DOF parafoil model but included the ability to easily model changing canopy incidence for additional control [10]. Separation of the parafoil and payload by a confluence point allows the payload to freely rotate with respect to the canopy resulting in 9 DOF. Doherr and Schilling reported on the development of a 9-DOF dynamic model for a rotating parachute [11]. By comparing results from 6- and 9-DOF models, they conclude a 9-DOF model was needed to adequately predict stability. Later, both Slegers and Costello [12] then Mooij et al. [13] developed 9-DOF models for parafoil systems using different approaches. Slegers and Costello [12] used Newtonian dynamics to form the equations of motion resulting in the internal constraint forces at the parafoil and payload connection being automatically solved during simulation. Mooij et al. [13] used analytical dynamics requiring artificial constraint stabilization to satisfy the constraint at the connection point. Strictly speaking, many payloads are not attached by an ideal confluence point, but rather by links that constrain the parafoil and payload roll to be the same. Modeling of such a system can be achieved using an 8-DOF model [14]. Müller et al. reported on an 8-DOF model used to evaluate simple maneuvers such as symmetric braking, wind gusts, and payload twist [15]. More recently, Redelinghuys [16] developed an 8-DOF model using analytical dynamics similar to Mooij et al. [13], which also requires artificial constraint stabilization. Constraint stabilization requires the addition of differential equations that artificially force the known constraints to be approximately satisfied. The constraint equations also require stabilization coefficients to be selected so these equations are stable. A tradeoff often exists between how close the constraint is met and stability of the constraint equations.

Parafoil and payload relative motion is important because, although the most significant loads come from the canopy, the payload is where sensors are located. Strickert and Jann attempted to measure the relative motion of a parafoil and payload using video-image processing [17]. Results were limited to post-flight-analysis due to the requirements of video digitization and synchronization. Differences in the orientation of the payload and canopy can make estimation of the canopy orientation and aerodynamic angles in real-time difficult. This paper develops an 8-DOF model that accurately models the relative motion of the payload with respect to the parafoil. Newtonian dynamics are used so that the constraint forces and moment are found analytically rather than using artificial constraint stabilization. The proposed model includes the coupling of translation and rotation dynamics from apparent mass. In addition, the change of canopy orientation with respect to the suspension lines is allowed similar to [10]. Finally, the proposed model is used to evaluate the effect of payload motion on guidance during a 180 deg turn common during terminal guidance in precision placement algorithms.

II. Eight-Degree-of-Freedom Dynamic Model

With the exception of movable parafoil brakes, the parafoil canopy is considered to be a fixed shape once it has completely inflated. The combined system of the parafoil canopy and the payload are modeled with 8 DOF, including three inertial position components of the point C (x_C, y_C, z_C), which is the midpoint of the parafoil-payload connection line, three Euler orientation angles of the parafoil system (φ_B, θ_B, ψ_B), and two Euler orientation angles of the payload with respect to the canopy (θ_S, ψ_S). Side and front views of the parafoil and payload system are shown in Figs. 1 and 2.

A body frame B is fixed at the mass center of the parafoil system, which includes the canopy, suspension lines, and risers with the $\vec{I}_B$ and $\vec{K}_B$ axes in the canopy plane of symmetry. Orientation of the body frame B with respect to the inertial frame I is obtained by a sequence of three body-fixed rotations. Starting from the inertial frame, the parafoil system is successively rotated through Euler yaw ψ_B, pitch θ_B, and roll φ_B. A payload frame S is fixed at the mass center of the payload. The payload orientation is also obtained by a sequence of body-fixed rotations. Starting from the body frame, the payload is rotated successively by the Euler yaw ψ_s then pitch θ_s. Transformations from the inertial to body frame and from the body to payload frame can be written as

$$T_{IB} = \begin{bmatrix} c_{\theta_B} c_{\psi_B} & c_{\theta_B} s_{\psi_B} & -s_{\theta_B} \\ s_{\phi_B} s_{\theta_B} c_{\psi_B} - c_{\phi_B} s_{\psi_B} & s_{\phi_B} s_{\theta_B} s_{\psi_B} + c_{\phi_B} c_{\psi_B} & s_{\phi_B} c_{\theta_B} \\ c_{\phi_B} s_{\theta_B} c_{\psi_B} + s_{\phi_B} s_{\psi_B} & c_{\phi_B} s_{\theta_B} s_{\psi_B} - s_{\phi_B} c_{\psi_B} & c_{\phi_B} c_{\theta_B} \end{bmatrix} \quad (1)$$

$$T_{BS} = \begin{bmatrix} c_{\theta_S} c_{\psi_S} & c_{\theta_S} s_{\psi_S} & -s_{\theta_S} \\ -s_{\psi_S} & c_{\psi_S} & 0 \\ s_{\theta_S} c_{\psi_S} & s_{\theta_S} s_{\psi_S} & c_{\theta_S} \end{bmatrix} \quad (2)$$

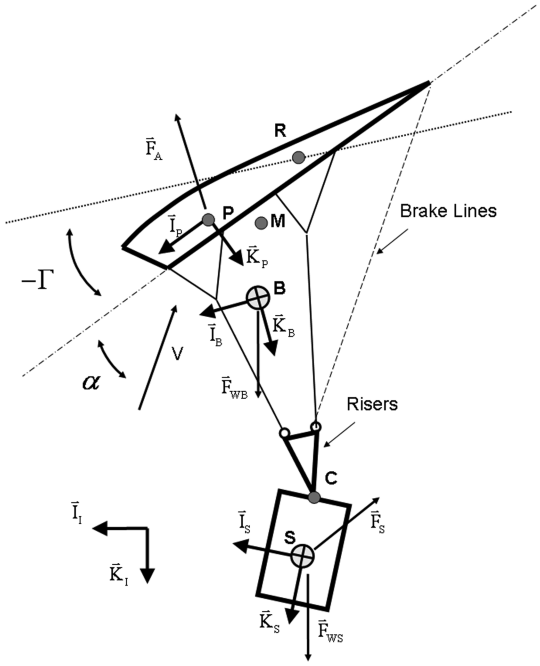

Fig. 1 Parafoil and payload side view.

where the common shorthand notation for trigonometric functions is employed with $\sin(\alpha) \equiv s_\alpha$, $\cos(\alpha) \equiv c_\alpha$, and $\tan(\alpha) \equiv t_\alpha$.

A parafoil canopy frame P is fixed to the canopy aerodynamic center. Orientation of the parafoil canopy frame with respect to the body frame is defined as the incidence angle Γ, and can be considered either a constant for the system or a control variable as in [10]. Rotation of the canopy about any point R fixed to the canopy allows tilting of the canopy lift and drag vectors resulting in changes in the equilibrium glide slope. For convenience, the notation $\vec{r}_{XY}$ is used for any position vector from a point X to a point Y with its components expressed in a specific frame. Using this notation, $\vec{r}_{CR}$ is the position vector from C to the canopy rotation point R, expressed in the body frame, and $\vec{r}_{RP}$ is the vector from the canopy rotation point R to the aerodynamic center P, expressed in the parafoil canopy frame.

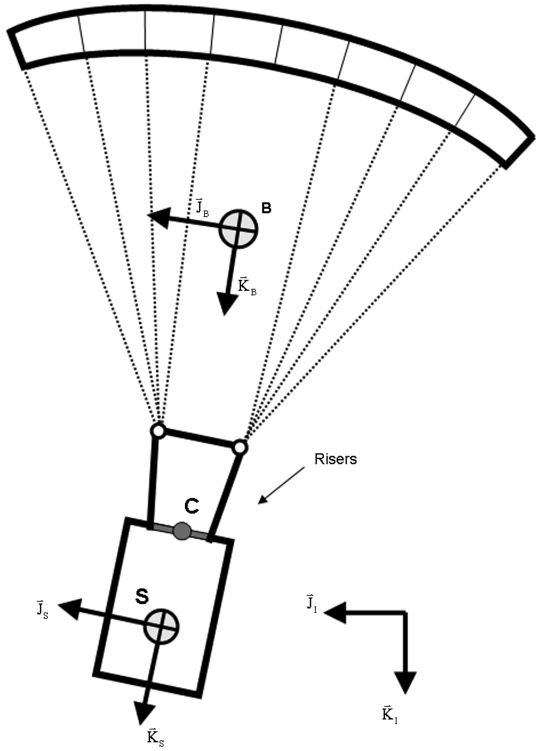

Fig. 2 Parafoil and payload front view.

A. Kinematics and Dynamics

The velocity vector components of point C are defined in the body frame leading to the translation kinematic differential equations:

$$\begin{Bmatrix} \dot{x}_C \\ \dot{y}_C \\ \dot{z}_C \end{Bmatrix} = [T_{IB}]^T \begin{Bmatrix} u_C \\ v_C \\ w_C \end{Bmatrix} \tag{3}$$

The angular velocity expressions for the parafoil body and payload with respect to the inertial frames are defined in Eqs. (4) and (5), respectively,

$$\vec{\omega}_{B/I} = p_B \vec{I}_B + q_B \vec{J}_B + r_B \vec{K}_B \tag{4}$$

$$\vec{\omega}_{S/I} = p_S \vec{I}_S + q_S \vec{J}_S + r_S \vec{K}_S \tag{5}$$

With these definitions, the rotation kinematics for the parafoil body become

$$\begin{Bmatrix} \dot{\phi}_B \\ \dot{\theta}_B \\ \dot{\psi}_B \end{Bmatrix} = \begin{bmatrix} 1 & s_{\phi_B} t_{\theta_B} & c_{\phi_B} t_{\theta_B} \\ 0 & c_{\phi_B} & -s_{\phi_B} \\ 0 & s_{\phi_B}/c_{\theta_B} & c_{\phi_B}/c_{\theta_B} \end{bmatrix} \begin{Bmatrix} p_B \\ q_B \\ r_B \end{Bmatrix} \tag{6}$$

and the two payload rotation kinematics equations, along with the constraint on the payload body roll rate, are given as

$$\begin{Bmatrix} p_S \\ \dot{\theta}_S \\ \dot{\psi}_S \end{Bmatrix} = \begin{bmatrix} 0 & -t_{\theta_S} \\ 1 & 0 \\ 0 & 1/c_{\theta_S} \end{bmatrix} \begin{Bmatrix} q_s \\ r_s \end{Bmatrix} + \begin{bmatrix} c_{\psi_S}/c_{\theta_S} & s_{\psi_S}/c_{\theta_S} & 0 \\ s_{\psi_S} & -c_{\psi_S} & 0 \\ -t_{\theta_S} c_{\psi_S} & -t_{\theta_S} s_{\psi_S} & -1 \end{bmatrix} \begin{Bmatrix} p_B \\ q_B \\ r_B \end{Bmatrix} \tag{7}$$

with a derivation provided in the Appendix.

Translation and rotation dynamic equations of motion are formed by separating the parafoil body and payload at the connection exposing the constraint forces and moments. Four vector equations can be formed, two by equating the time derivative of linear momentum with total forces on each body, and two more by equating the time derivative of angular momentum with the total moment on each body. The required mass center accelerations of the parafoil and payload are

$$\vec{a}_{B/I} = \begin{Bmatrix} \dot{u}_C \\ \dot{v}_C \\ \dot{w}_C \end{Bmatrix} + S^B_{\omega_B} \begin{Bmatrix} u_C \\ v_C \\ w_C \end{Bmatrix} - S^B_{r_{CB}} \begin{Bmatrix} \dot{p}_B \\ \dot{q}_B \\ \dot{r}_B \end{Bmatrix} + S^B_{\omega_B} S^B_{\omega_B} \begin{Bmatrix} x_{CB} \\ y_{CB} \\ z_{CB} \end{Bmatrix} \tag{8}$$

$$\vec{a}_{S/I} = [T_{BS}] \left(\begin{Bmatrix} \dot{u}_C \\ \dot{v}_C \\ \dot{w}_C \end{Bmatrix} + S^B_{\omega_B} \begin{Bmatrix} u_C \\ v_C \\ w_C \end{Bmatrix} \right) - S^S_{r_{CS}} \begin{Bmatrix} \dot{p}_S \\ \dot{q}_S \\ \dot{r}_S \end{Bmatrix} + S^S_{\omega_S} S^S_{\omega_S} \begin{Bmatrix} x_{CS} \\ y_{CS} \\ z_{CS} \end{Bmatrix} \tag{9}$$

where each acceleration is expressed in its respective frame. The vectors $\vec{r}_{CB}$ and $\vec{r}_{CS}$ are position vectors from C to the parafoil body and payload mass centers, both expressed in their respective frames. The convention is used where the vector cross product of two vectors $\vec{r} = \{ r_x \quad r_y \quad r_z \}^T$ and $\vec{F} = \{ F_x \quad F_y \quad F_z \}^T$ both expressed in the A reference frame is written as

$$S_r^A \vec{F} = \begin{bmatrix} 0 & -r_z & r_y \\ r_z & 0 & -r_x \\ -r_y & r_x & 0 \end{bmatrix} \begin{Bmatrix} F_x \\ F_y \\ F_z \end{Bmatrix} \tag{10}$$

The derivative of angular momentum for the parafoil body and payload can be expressed in their respective frames:

$$\frac{\mathrm{d}}{\mathrm{d}t}\vec{H}_{B/I} = [I_B]\begin{Bmatrix} \dot{p}_B \\ \dot{q}_B \\ \dot{r}_B \end{Bmatrix} + S^B_{\omega_B}[I_B]\begin{Bmatrix} p_B \\ q_B \\ r_B \end{Bmatrix} \tag{11}$$

$$\frac{\mathrm{d}}{\mathrm{d}t}\vec{H}_{S/I} = [I_S]\begin{Bmatrix} \dot{p}_S \\ \dot{q}_S \\ \dot{r}_S \end{Bmatrix} + S^S_{\omega_S}[I_S]\begin{Bmatrix} p_S \\ q_S \\ r_S \end{Bmatrix} \tag{12}$$

Notice that the derivative of p_S appears in both Eqs. (9) and (12), but is known through the kinematic constraint in the first row of Eq. (7). Differentiating p_S enables the angular acceleration of the payload to be written in the compact form

$$\begin{Bmatrix} \dot{p}_S \\ \dot{q}_S \\ \dot{r}_S \end{Bmatrix} = \mathbf{G_1} + \mathbf{K_1}\begin{Bmatrix} \dot{q}_S \\ \dot{r}_S \end{Bmatrix} + \mathbf{K}_2\begin{Bmatrix} \dot{p}_B \\ \dot{q}_B \\ \dot{r}_B \end{Bmatrix} \tag{13}$$

where

$$\begin{aligned} g_1 = {} & (1/c^2_{\theta_S})[s_{\theta_S}(c_{\psi_S}p_B + s_{\psi_S}q_B)q_S + 2(c_{\psi_S}q_B - s_{\psi_S}p_B)r_S \\ & - q_S r_S + c_{\theta_S}(s_{\psi_S}p_B - c_{\psi_S}q_B)r_B + 2s_{\theta_S}s_{\psi_S}c_{\psi_S}(p_B^2 - q_B^2) \\ & + 2p_B q_B s_{\theta_S}(s^2_{\psi_S} - c^2_{\psi_S})] \end{aligned} \tag{14}$$

$$\mathbf{G_1} = \begin{Bmatrix} g_1 \\ 0 \\ 0 \end{Bmatrix} \tag{15}$$

$$\mathbf{K_1} = \begin{bmatrix} 0 & -t_{\theta_S} \\ 1 & 0 \\ 0 & 1 \end{bmatrix} \tag{16}$$

$$\mathbf{K_2} = \begin{bmatrix} c_{\psi_S}/c_{\theta_S} & s_{\psi_S}/c_{\theta_S} & 0 \\ 0 & 0 & 0 \\ 0 & 0 & 0 \end{bmatrix} \tag{17}$$

The known derivative of p_S can be eliminated from the mass center acceleration and derivative of angular momentum of the payload by using Eq. (13). The resulting expressions for the mass center acceleration and derivative of angular momentum of the payload can then be written as

$$\begin{aligned} \vec{a}_{S/I} = {} & [T_{BS}]\left(\begin{Bmatrix} \dot{u}_C \\ \dot{v}_C \\ \dot{w}_C \end{Bmatrix} + S^B_{\omega_B}\begin{Bmatrix} u_C \\ v_C \\ w_C \end{Bmatrix}\right) - S^S_{r_{CS}}\mathbf{G_1} - S^S_{r_{CS}}\mathbf{K_1}\begin{Bmatrix} \dot{q}_S \\ \dot{r}_S \end{Bmatrix} \\ & - S^S_{r_{CS}}\mathbf{K_2}\begin{Bmatrix} \dot{p}_B \\ \dot{q}_B \\ \dot{r}_B \end{Bmatrix} + S^S_{\omega_S}S^S_{\omega_S}\begin{Bmatrix} x_{CS} \\ y_{CS} \\ z_{CS} \end{Bmatrix} \end{aligned} \tag{18}$$

$$\frac{\mathrm{d}}{\mathrm{d}t}\vec{H}_{S/I} = [I_S]\mathbf{G_1} + [I_S]\mathbf{K_1}\begin{Bmatrix} \dot{q}_S \\ \dot{r}_S \end{Bmatrix} + [I_S]\mathbf{K_2}\begin{Bmatrix} \dot{p}_B \\ \dot{q}_B \\ \dot{r}_B \end{Bmatrix} + S^S_{\omega_S}[I_S]\begin{Bmatrix} p_S \\ q_S \\ r_S \end{Bmatrix} \tag{19}$$

where both quantities are expressed in terms of only states and state derivatives.

B. Forces and Moments

1. Weight Contribution

Forces and moments acting on the parafoil and payload have contributions from weight, aerodynamic loads on the canopy and payload, apparent mass of the canopy, constraint forces at the connection, and constraint moments at the connection. Weight contributions of the parafoil system and payload are expressed in their respective frames as

$$\vec{F}_{WB} = m_B g\begin{Bmatrix} -s_{\theta_B} \\ s_{\phi_B}c_{\theta_B} \\ c_{\phi_B}c_{\theta_B} \end{Bmatrix} \tag{20}$$

$$\vec{F}_{WS} = m_s g[T_{BS}]\begin{Bmatrix} -s_{\theta_B} \\ s_{\phi_B}c_{\theta_B} \\ c_{\phi_B}c_{\theta_B} \end{Bmatrix} \tag{21}$$

2. Aerodynamic Forces

Aerodynamic forces on the canopy are expressed in the body reference frame; however, they are a function of the aerodynamics velocities in the canopy frame. Defining T_{BP} as the single axis transformation from the body to canopy reference frame by the incidence angle Γ, the aerodynamic velocity of the canopy expressed in the canopy frame is written as

$$\begin{aligned} \begin{Bmatrix} \tilde{u} \\ \tilde{v} \\ \tilde{w} \end{Bmatrix} = {} & [T_{BP}]\left(\begin{Bmatrix} u_C \\ v_C \\ w_C \end{Bmatrix} + S^B_{\omega_B}\left(\begin{Bmatrix} x_{CR} \\ y_{CR} \\ z_{CR} \end{Bmatrix} + [T_{BP}]^T\begin{Bmatrix} x_{RP} \\ y_{RP} \\ z_{RP} \end{Bmatrix}\right)\right. \\ & \left. - [T_{IB}]\vec{V}_{A/I}\right) \end{aligned} \tag{22}$$

The aerodynamic angles then become $\alpha = \mathrm{atan}\,(\tilde{w}/\tilde{u})$ and $\beta = \mathrm{asin}\,(\tilde{v}/V_A)$ where $V_A = \sqrt{\tilde{u}^2 + \tilde{v}^2 + \tilde{w}^2}$. Canopy aerodynamic forces in the body reference frame can then be written as

$$\vec{F}_A = \frac{1}{2}\rho V_A^2 S_P [T_{BP}]^T[T_{AP}]\begin{Bmatrix} C_{D0} + C_{D\alpha^2}\alpha^2 \\ C_{Y\beta}\beta \\ C_{L0} + C_{L\alpha}\alpha \end{Bmatrix} \tag{23}$$

where T_{AP} is the transformation from the aerodynamic to canopy frames by the angle α. Payload drag is defined in a similar manner,

$$\vec{F}_S = -\frac{1}{2}\rho V_S S_S C_{DS}\begin{Bmatrix} u_{SA} \\ v_{SA} \\ w_{SA} \end{Bmatrix} \tag{24}$$

where u_{SA}, v_{SA}, and w_{SA} are payload aerodynamic velocities in the payload frame and $V_S = \sqrt{\tilde{u}_{SA}^2 + \tilde{v}_{SA}^2 + \tilde{w}_{SA}^2}$. Unsteady aerodynamic moments on the canopy expressed in the body frame are given in Eq. (25):

$$\vec{M}_A = \frac{1}{2}\rho V_A^2 S_P [T_{BP}]^T\begin{Bmatrix} b((b/2V_A)C_{lp}\tilde{p} + C_{l\delta a}\delta_a) \\ \bar{c}(C_{m0} + (\bar{c}/2V_A)C_{mq}\tilde{q}) \\ b((b/2V_A)C_{nr}\tilde{r} + C_{n\delta a}\delta_a) \end{Bmatrix} \tag{25}$$

3. Apparent Mass

Parafoil canopies with small mass-to-volume ratios can experience large forces and moments from accelerating fluid called apparent mass and apparent inertia. They appear as additional mass and inertia values in the final equations of motion, provided that their effects are not already covered by the aerodynamic coefficients. Parafoil canopies with small arch-to-span ratios and negligible camber can be approximated to useful accuracy by an ellipsoid having three planes of symmetry. Approximation of the canopy as an ellipsoid allows the kinetic energy of the fluid displaced by its movement to be written as [18]

$$2T = A\tilde{u}^2 + B\tilde{v}^2 + C\tilde{w}^2 + P\tilde{p}^2 + Q\tilde{q}^2 + R\tilde{r}^2 \tag{26}$$

where velocities of the canopy $\tilde{u}, \tilde{v}, \tilde{w}$ expressed in the canopy frame were previously defined in Eq. (22) and the angular velocities of the canopy also expressed in the canopy frame $\tilde{p}, \tilde{q}, \tilde{r}$ are defined as

$$\begin{Bmatrix} \tilde{p} \\ \tilde{q} \\ \tilde{r} \end{Bmatrix} = [T_{BP}] \begin{Bmatrix} p_B \\ q_B \\ r_B \end{Bmatrix} \tag{27}$$

where it is assumed that Γ is either constant or slowly changing compared to the system dynamics. Constants A, B, C, P, Q, and R appearing in Eq. (26) can be calculated for known simple shapes or can be approximated as discussed in [7,9,18]. Similar to Lissaman and Brown [7], forces and moments from apparent mass and inertia are found by relating the fluid's kinetic energy to resultant forces and moments. Assuming the incidence angle Γ is slowly varying or constant, so that its derivative is negligible, the apparent mass contributions expressed in the body frame can be written as

$$\vec{F}_{\mathrm{AM}} = -[T_{BP}]^T \left([I_{\mathrm{AM}}] \begin{Bmatrix} \dot{\tilde{u}} \\ \dot{\tilde{v}} \\ \dot{\tilde{w}} \end{Bmatrix} + S^P_{\omega_B} [I_{\mathrm{AM}}] \begin{Bmatrix} \tilde{u} \\ \tilde{v} \\ \tilde{w} \end{Bmatrix} \right) \tag{28}$$

$$\vec{M}_{\mathrm{AM}} = -[T_{BP}]^T \left([I_{\mathrm{AI}}] \begin{Bmatrix} \dot{\tilde{p}} \\ \dot{\tilde{q}} \\ \dot{\tilde{r}} \end{Bmatrix} + S^P_{\omega_B} [I_{\mathrm{AI}}] \begin{Bmatrix} \tilde{p} \\ \tilde{q} \\ \tilde{r} \end{Bmatrix} \right) \tag{29}$$

where effects already covered by the aerodynamic coefficients connected to steady or quasi-steady motions have been excluded and

$$[I_{\mathrm{AM}}] = \begin{bmatrix} A & 0 & 0 \\ 0 & B & 0 \\ 0 & 0 & C \end{bmatrix} \tag{30}$$

$$[I_{\mathrm{AI}}] = \begin{bmatrix} P & 0 & 0 \\ 0 & Q & 0 \\ 0 & 0 & R \end{bmatrix} \tag{31}$$

Apparent mass forces and moments act at the apparent mass center shown as (M) in Fig. 1. For the assumed ellipsoidal canopy shape, the apparent mass center occurs at approximately the canopy centroid.

4. Constraint Forces and Moments

Constraint forces and moments expressed in the body frame are defined as

$$\vec{F}_C = \{ F_{CX} \quad F_{CY} \quad F_{CZ} \}^T \tag{32}$$

$$\vec{M}_C = \mathbf{E}_1 M_{CX} + \mathbf{E_3} M_{CZ} \tag{33}$$

where F_{CX}, F_{CY}, and F_{CZ} are the unknown components of the constraint force at the connection, M_{CX} is the unknown roll constraint moment at the connection, M_{CZ} is any known twisting moment from a line twist model, and $\mathbf{E}_i$ is a 3×1 column vector with a one on the ith element and zeros everywhere else. The line twist moment M_{CZ} is dependent on the specific payload-canopy connection and riser geometry and can vary dramatically from system to system. In general, the line twist moment M_{CZ} can be modeled as a nonlinear rotational spring and damper where both the stiffness K_ψ and damping coefficient K_r are functions of ψ_S

$$M_{CZ} = K_\psi(\psi_S)\psi_S + K_r(\psi_S) r_S \tag{34}$$

C. Equations of Motion

Coupling of the translation and rotation dynamics make algebraic elimination of the unknown constraint forces (F_{CX}, F_{CY}, F_{CZ}) and moment M_{CX} from the final equations difficult. Therefore, they are not eliminated and, as a consequence, the constraint forces (F_{CX}, F_{CY}, F_{CZ}) and moment M_{CX} are found during the numerical solution along with the model states. Final dynamic equations of motion and the unknown constraints can be expressed compactly in matrix form:

$$\begin{bmatrix} -m_S S^S_{r_{CS}} \mathbf{K_1} & -m_S S^S_{r_{CS}} \mathbf{K_2} & m_S T_{BS} & -T_{BS} & \mathbf{0_{3\times1}} \\ \mathbf{0_{3\times2}} & -I'_{\mathrm{AM}} S^B_{r_{CM}} - (m_B + m_I) S^B_{r_{CB}} & (m_B + m_I)\mathbf{I_{3\times3}} + I'_{\mathrm{AM}} & \mathbf{I_{3\times3}} & \mathbf{0_{3\times1}} \\ I_S \mathbf{K_1} & I_S \mathbf{K_2} & \mathbf{0_{3\times3}} & S^S_{r_{CS}} T_{BS} & -T_{BS}\mathbf{E_1} \\ \mathbf{0_{3\times2}} & I_B + I'_{\mathrm{AI}} - S^B_{r_{BM}} I'_{\mathrm{AM}} S^B_{r_{CM}} & S^B_{r_{BM}} I'_{\mathrm{AM}} & -S^B_{r_{CB}} & \mathbf{E_1} \end{bmatrix} \begin{Bmatrix} \dot{q}_S \\ \dot{r}_S \\ \cdots \\ \dot{p}_B \\ \dot{q}_B \\ \dot{r}_B \\ \cdots \\ \dot{u}_C \\ \dot{v}_C \\ \dot{w}_C \\ \cdots \\ F_{CX} \\ F_{CY} \\ F_{CZ} \\ \cdots \\ M_{CX} \end{Bmatrix} = \begin{Bmatrix} \mathbf{B_1} \\ \cdots \\ \mathbf{B_2} \\ \cdots \\ \mathbf{B_3} \\ \cdots \\ \mathbf{B_4} \end{Bmatrix} \tag{35}$$

$$\mathbf{B_1} = \vec{F}_S + \vec{F}_{WS} - m_S T_{BS} S^B_{\omega_B} \begin{Bmatrix} u_C \\ v_C \\ w_C \end{Bmatrix} + m_S S^S_{r_{CS}} \mathbf{G_1} - m_S S^S_{\omega_S} S^S_{\omega_S} \begin{Bmatrix} x_{CS} \\ y_{CS} \\ z_{CS} \end{Bmatrix} \tag{36}$$

$$\mathbf{B_2} = \vec{F}_A + \vec{F}_{WB} - (m_B + m_I) S^B_{\omega_B} \begin{Bmatrix} u_C \\ v_C \\ w_C \end{Bmatrix} - (m_B + m_I) S^B_{\omega_B} S^B_{\omega_B} \begin{Bmatrix} x_{CB} \\ y_{CB} \\ z_{CB} \end{Bmatrix} - [T_{BP}]^T S^B_{\omega_B} I_{\mathrm{AM}} \begin{Bmatrix} \tilde{u} \\ \tilde{v} \\ \tilde{w} \end{Bmatrix} - I'_{\mathrm{AM}} S^B_{\omega_B} T_{IB} \vec{V}_{A/I} \tag{37}$$

$$\mathbf{B_3} = -I_S \mathbf{G_1} - S^S_{\omega_S} I_S \begin{Bmatrix} p_S \\ q_S \\ r_S \end{Bmatrix} + T_{BS} \begin{Bmatrix} 0 \\ 0 \\ M_{CZ} \end{Bmatrix} \tag{38}$$

$$\mathbf{B}_4 = \vec{M}_A + S^B_{r_{BP}}\vec{F}_A - S^B_{r_{BM}}[T_{BP}]^T S^P_{\omega_B} I_{\mathrm{AM}} \begin{Bmatrix} \tilde{u} \\ \tilde{v} \\ \tilde{w} \end{Bmatrix} - [T_{BP}]^T S^P_{\omega_B} I_{\mathrm{AI}} \begin{Bmatrix} \tilde{p} \\ \tilde{q} \\ \tilde{r} \end{Bmatrix} - S^B_{\omega_B} I_B \begin{Bmatrix} p_B \\ q_B \\ r_B \end{Bmatrix} - \begin{Bmatrix} 0 \\ 0 \\ M_{CZ} \end{Bmatrix} - S^B_{r_{BM}} I'_{\mathrm{AM}} S^B_{\omega_B} T_{IB} \vec{V}_{A/I} \tag{39}$$

where $\vec{r}_{BP}$ and $\vec{r}_{BM}$ are position vectors from the body mass center to the canopy aerodynamic center and apparent mass center, both expressed in the body frame. The first and second sets of row equations appearing in Eq. (35) are found by summing forces on the payload and parafoil. The third and fourth sets of row equations appearing in Eq. (35) are found by summing moments about the payload and parafoil mass centers. The common convention is used for tensors of second rank such that $I'_X = [T_{BP}]^T[I_X][T_{BP}]$ for the quantities in Eqs. (30) and (31). Derivatives of the eight states and four constraints are found by solving the system of equations in Eq. (35) using LU decomposition. Combining the eight state derivatives with the eight kinematic equations in Eqs. (3), (6), and (7) results in 16 differential equations representing the 8-DOF parafoil and payload model.

III. Results

The equations of motion previously described are numerically integrated to generate the trajectory using a fourth-order Runge–Kutta algorithm with time step of 0.005 s. Simulations under two sets of conditions are performed so that the response of the parafoil and payload system can be evaluated. The first simulation evaluates the relative motion of the payload with respect to the parafoil for a commanded brake deflection. Simulations in the second case evaluate the performance of a simple yaw controller for different levels of resistance to line twist. In both cases, the simulation is started at zero cross range and down range, from 2500 ft above sea level, with payload and parafoil pitch angles of −1.0 and −2.0 deg, u_C being 28.2 ft/s, w_C being 14.0 ft/s, and all other states zero.

The payload is rectangular with a drag area of 0.45 ft^2, a depth of 0.4 ft, and a weight of 4.25 lbf. The parafoil canopy and suspension lines have a combined weight of 0.5 lbf. The canopy has a span of 4.25 ft, mean chord of 2.5 ft, Γ of −12 deg, and maximum control deflection of 0.75 ft. All aerodynamic coefficients and apparent mass coefficients for the canopy are provided in Table 1. Aerodynamic coefficients were estimated from flights of a small experimental system in a similar manner to [3,10]. It is noted that the coefficients in Table 1 for the small parafoil are somewhat similar to those used and reported for bigger systems [19]. Inertia matrices for both the parafoil and payload are provided next, both having units of slug-ft^2:

Table 1 Parafoil and payload physical parameters

Parameter	Value	Units
C_{D0}	0.15	——
$C_{D\alpha^2}$	0.90	——
$C_{Y\beta}$	−0.05	——
C_{L0}	0.25	——
$C_{L\alpha}$	0.68	——
C_{lp}	−0.355	——
$C_{l\delta a}$	−0.00032	——
C_{m0}	0.0	——
C_{mq}	−0.265	——
C_{nr}	−0.09	——
$C_{n\delta a}$	0.0059	——
C_{DS}	0.40	——
A	0.0008	slug
B	0.0022	slug
C	0.0290	slug
P	0.040	slug · ft^2
Q	0.010	slug · ft^2
R	0.0018	slug · ft^2

$$I_B = \begin{bmatrix} 0.031 & 0 & -0.005 \\ 0 & 0.020 & 0 \\ -0.005 & 0 & 0.040 \end{bmatrix} \tag{40}$$

$$I_S = \begin{bmatrix} 0.312 & 0 & 0.022 \\ 0 & 0.296 & 0 \\ 0.022 & 0 & 0.049 \end{bmatrix} \tag{41}$$

Vectors from the point C to the payload mass center, parafoil mass center, and canopy rotation point are as follows: $\vec{r}_{CS} = 1.0\vec{K}_S$ ft, $\vec{r}_{CB} = 0.5\vec{I}_B - 2.25\vec{K}_B$ ft, and $\vec{r}_{CR} = -0.5\vec{K}_B - 2.7\vec{K}_B$. Vectors from the canopy rotation point to the parafoil aerodynamic center and apparent mass center are $\vec{r}_{RP} = 0.63\vec{I}_P$ ft and $\vec{r}_{RM} = 0.590\vec{I}_P + 0.2\vec{K}_P$ ft, respectively. The rotational stiffness and damping from risers are assumed to be constant with values of 0.07 N-m/rad and 0.005 N-m-s/rad.

A. Response to a Constant Brake Deflection

Relative motion of the payload with respect to canopy is demonstrated using a commanded 50% left brake deflection from 10 to 18.5 s. The resulting path shown in Fig. 3 is a complete 180-deg

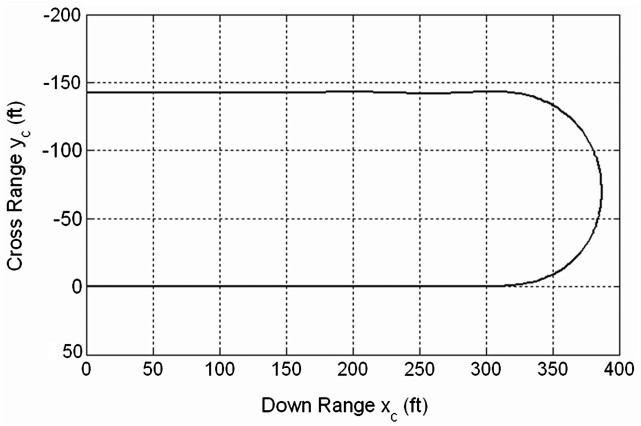

Fig. 3 Ground track from a 50% left brake deflection.

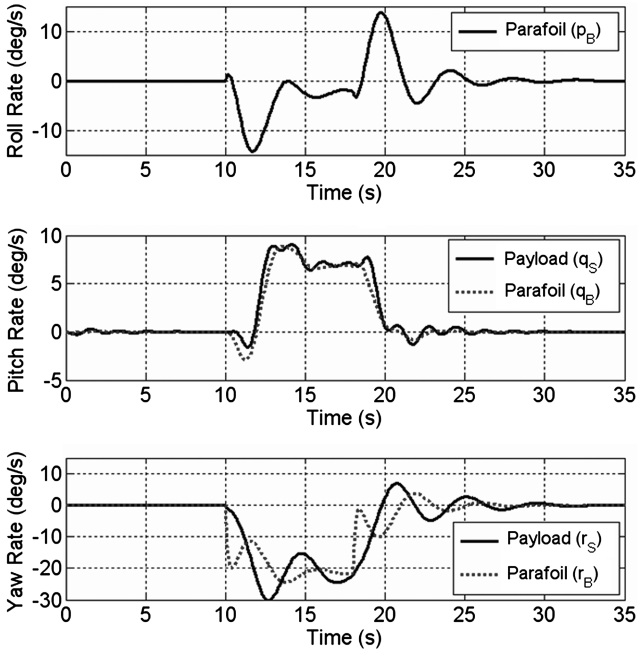

Fig. 4 Angular rates in response to a 50% left brake deflection.

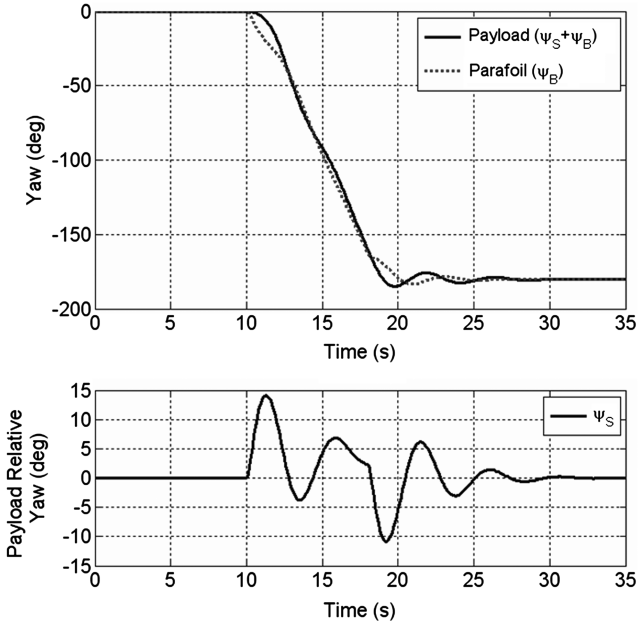

Fig. 5 System yaw angle response to a 50% left brake deflection.

turn common in precision placement algorithms. During the maneuver, the descent rate is a nearly constant 15.1 ft/s. Figure 4 shows the angular velocities of both the canopy and payload where the turn rate from a 50% brake is approximately -20 deg/s resulting in a turn diameter of 145 ft. Total and relative yawing motion of the payload and canopy is shown in Fig. 5. The left brake at 10 s first results in canopy yaw with the payload lagging behind by 15 deg. A similar response is observed when the left brake is later removed. After removal of brake deflection, the payload yaws with respect to the canopy for 10 s before the oscillation ceases. Roll and pitch angles as well as the canopy angle of attack and sideslip are shown in Figs. 6 and 7. The roll angle in Fig. 6 responds in a similar manner as yaw with both the frequency and damping being similar. As the canopy banks left during the turn, it also pitches down. Pitch of the payload and canopy are closely aligned as shown by the small pitch angle of the payload with respect to the canopy θ_S in Fig. 6. Pitching motion occurs at a higher frequency than both roll and yaw for the case shown, and is a function of the payload distance below the connection.

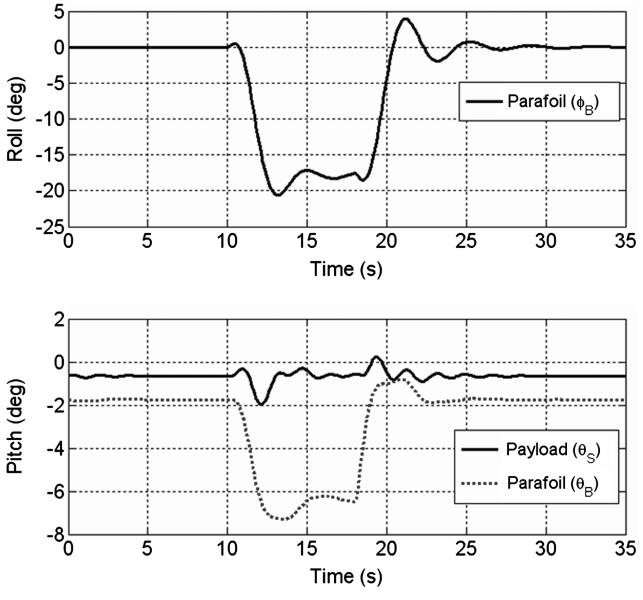

Fig. 6 System roll and pitch angles response to a 50% left brake deflection.

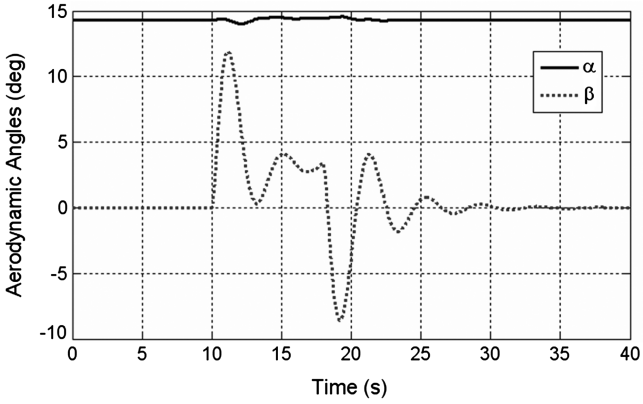

Fig. 7 Angle of attack and sideslip response to a 50% left brake deflection.

B. Control System Response

The previous open-loop turn command showed only moderate payload yawing motion with respect to the canopy. In practice, closed-loop turn commands are implemented using sensor feedback to improve robustness to disturbances and improve performance. Many systems only have sensors on the payload and no information about canopy orientation. A simple proportional-derivative controller is proposed to track a desired yaw command using a feed forward gain K_{FF}, a proportional gain K, and a derivative gain aK:

$$\delta_a = K_{\text{FF}}\dot{\psi}_{\text{DES}} - K[(\psi - \psi_{\text{DES}}) + a(r_S - \dot{\psi}_{\text{DES}})] \qquad (42)$$

The desired turn command ψ_{DES} is for the overall parafoil system; however, only the payload states $\psi = \psi_S + \psi_B$ and r_S are used in the control algorithm.

The desired command is taken to be a 180 deg left turn over 8.25 s. Two systems are compared. The first being the 8-DOF system in Figs. 3–7 with line twist stiffness and damping values of 0.07 N-m/rad and 0.005 N-m-s/rad. The second mimics a 7-DOF system by using large rotational stiffness and damping values of 10 N-m/rad and 1.0 N-m-s/rad. Large resistance to line twist results in trivial yawing motion of the payload with respect to the canopy. The second system will be referred to from here on as the 7-DOF system. Figures 8–10 show results for both the 7- and 8-DOF systems when $K_{\text{FF}} = 1.21$ s/rad, $K = 0.70$/rad, and $a = 0.5$ s. Relative motion of the payload in the 8-DOF system results in a persistent oscillation of cross range shown in Fig. 8, payload yaw shown in Fig. 9, and control deflection in Fig. 10. In contrast, the 7-DOF model, under the same control algorithm, results in good performance with little error and no control oscillations. In Fig. 9, the yaw of the payload and canopy are shown separately for the 8-DOF system, whereas, for

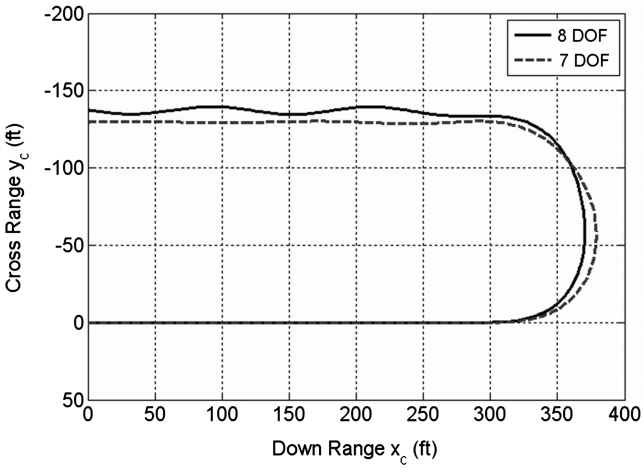

Fig. 8 Closed-loop ground track.

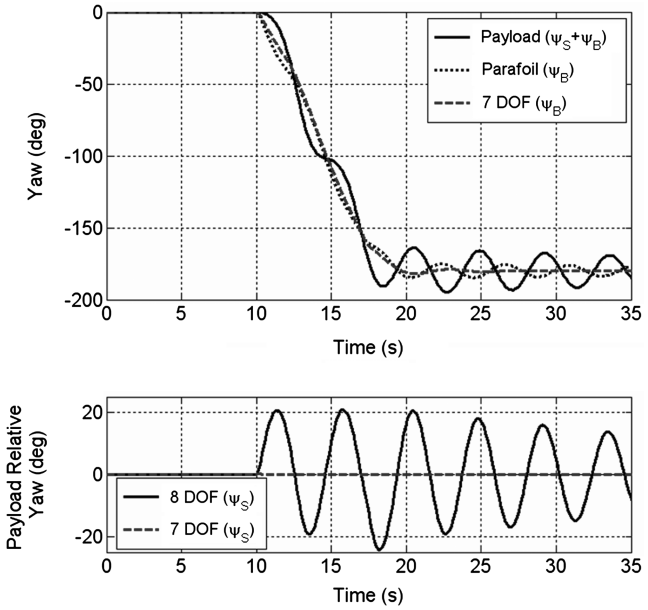

Fig. 9 Closed-loop payload and canopy yaw.

the 7-DOF system, yaw of both the payload and canopy are constrained by the large stiffness and are shown by a single line.

Reduction of the control gain K to 0.2/rad eliminates the persistent oscillation of the control deflection. However, as seen in Fig. 11, control response is sluggish. The payload in the 8-DOF system still has relative motion throughout the turn for a smaller gain K, but now decays after the turn as shown in Fig. 12. Reduction of the gain K also results in the closed-loop trajectory resembling the open-loop trajectory in Fig. 3.

A root locus for the 8-DOF system is shown in Fig. 13 where only the six poles significantly effected by the control gain K are given. The oscillatory response of the relative payload-canopy yaw ψ_S is dominated by the complex conjugate pair of poles that approach the imaginary axis as K is increased. As K increases, the mode's frequency remains near 0.24 Hz but the damping ratio decreases from 0.19 when K is zero to 0.17 and 0.03 for low and high gains.

Figures 8–10 demonstrate that a 7-DOF model may not accurately predict the closed-loop performance of a system that exhibits relative payload-canopy yawing. To predict the turn response of an 8-DOF model, a reduced-order four-state linear model is considered. States include the payload yaw ψ, canopy yaw ψ_B, payload yaw rate r_S, and

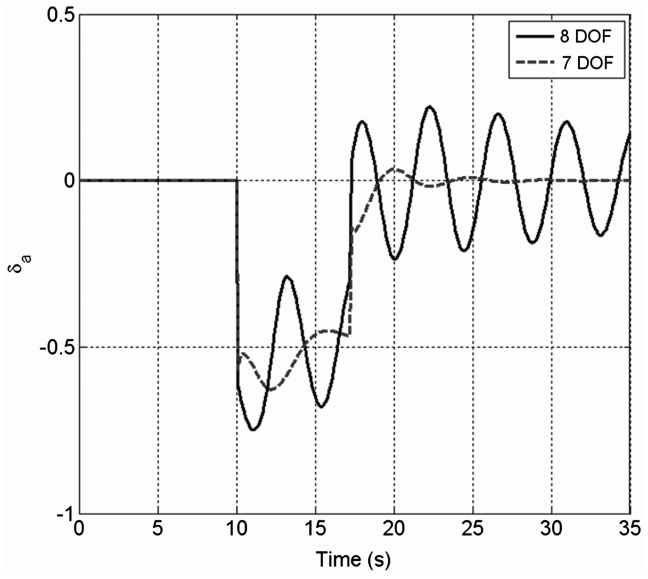

Fig. 10 Control deflection.

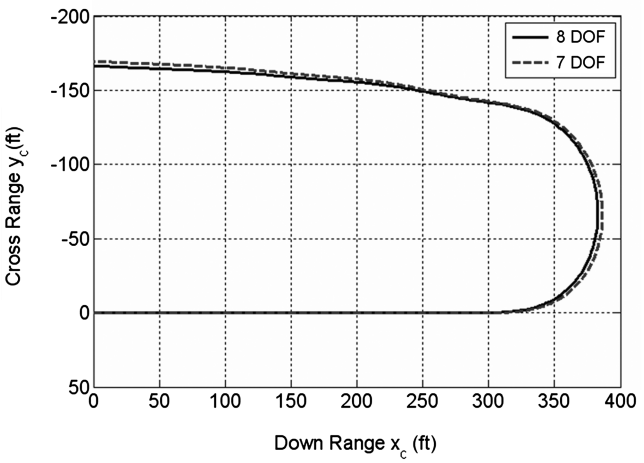

Fig. 11 Low-gain ground track.

canopy yaw rate r_B. Finite difference approximations are used to calculate a linear approximation which takes the form

$$\begin{Bmatrix} \dot{\psi} \\ \dot{\psi}_B \\ \dot{r}_S \\ \dot{r}_B \end{Bmatrix} = \begin{bmatrix} 0 & 0 & 1 & 0 \\ 0 & 0 & 0 & 1 \\ A_{31} & -A_{31} & A_{33} & A_{34} \\ A_{41} & -A_{41} & A_{43} & A_{44} \end{bmatrix} \begin{Bmatrix} \psi \\ \psi_B \\ r_S \\ r_B \end{Bmatrix} + \begin{Bmatrix} 0 \\ 0 \\ 0 \\ B_4 \end{Bmatrix} \delta_a \quad (43)$$

where, for the previous 8-DOF system, A_{31}, A_{33}, and A_{34} are -1.72, -0.53, and -0.21; A_{41}, A_{43}, and A_{44} are 1.50, 0.09, and -7.72; and B_4 is 6.03. Using the proposed proportional-derivative controller in Eq. (42) with $a = 0.5$ s, the closed-loop dynamics predicted by the linear model are compared with those from 8-DOF simulations for different gains K. Figure 14 shows the simulated and predicted damping ratios ζ and frequency ratios μ, where μ is the ratio of the closed-loop natural frequency and the open-loop natural frequency. The linear model accurately predicts the persistent oscillations from low damping when K is 0.7 as well as the higher damping when K is 0.2. The reduced-order linear model provides a useful tool for analysis of the turn controller. From Fig. 14, a $K < 0.20$/rad results in a closed-loop damping ratio of greater than 74% of the open-loop system, achieving a similar ground track as the 7-DOF system where payload relative yawing motion was ignored. Figure 14 also predicts for the example system that a $K > 0.50$/rad results in a very low damping ratio (<23% of the open-loop damping ratio) where payload relative yawing motion cannot be ignored.

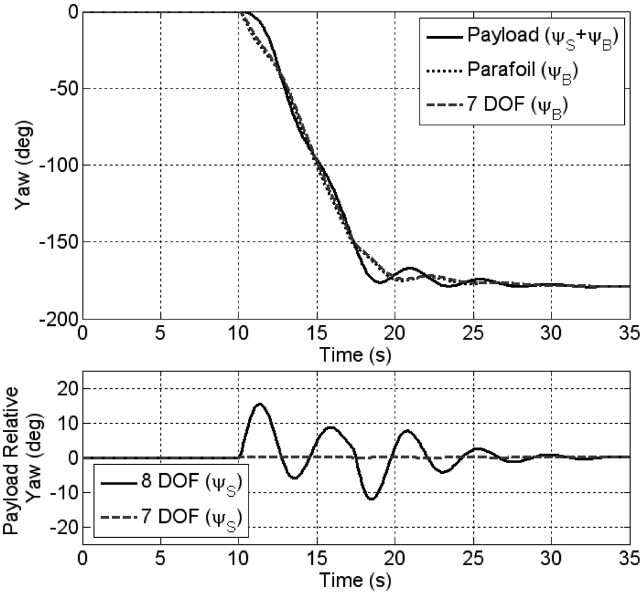

Fig. 12 Low-gain payload and canopy yaw.

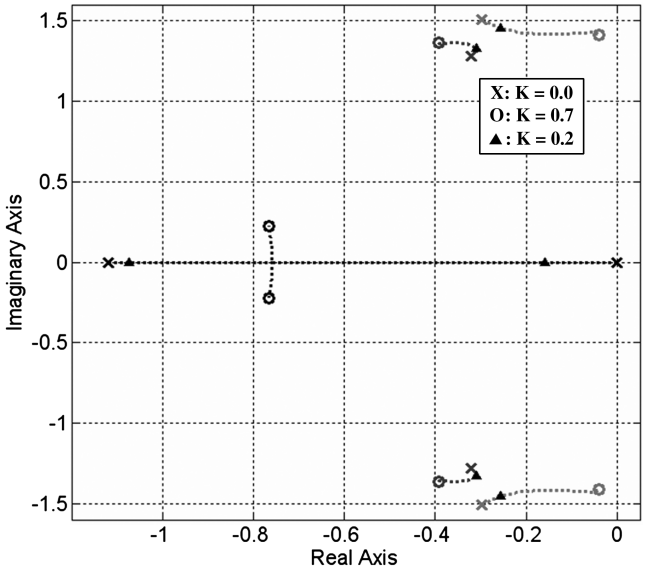

Fig. 13 Root locus for 8-DOF model with $a = 0.5$.

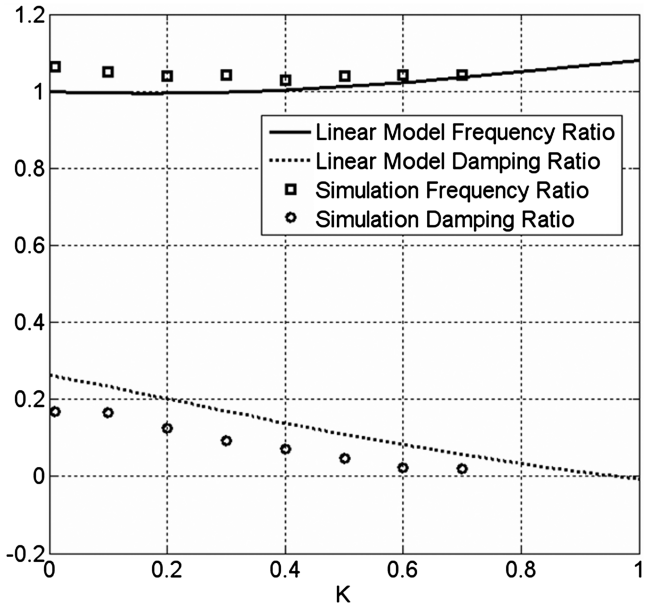

Fig. 14 Comparison of reduced linear model with simulated response.

IV. Conclusions

An 8-DOF model was developed that accurately models the relative motion of the payload with respect to a parafoil. Constraint forces and moment were found analytically rather than using artificial constraint stabilization, simplifying numerical solution of the equations of motion. It was shown through simulation that relative payload motion had little effect on the predicted ground track for a constant brake deflection. Addition of a closed-loop yaw controller, common in precision placement algorithms, demonstrated that, even when the relative motion of the payload is moderate, persistent yawing oscillations can occur, resulting in poor closed-loop performance. A 7-DOF model neglecting relative payload yawing failed to predict the same oscillations. Reduction of feedback gains reduced oscillations in both motion and control; however, resulting tracking performance was degraded. The 7-DOF model was able to model controller performance in a low-gain system despite ignoring relative yawing motion. Finally, it was shown that a reduced-order linear model was able to adequately predict the 8-DOF closed-loop damping of the yaw controller. The linear model provides a means of selecting feedback gains so that relative motion of the payload has little effect on the final ground track.

Appendix: Payload Rotation Kinematics

The angular velocity of the payload with respect to the parafoil $\vec{\omega}_{S/B}$ with components expressed in the payload frame S can be written two ways. First, $\vec{\omega}_{S/B}$ can be written as

$$\vec{\omega}_{S/B} = \vec{\omega}_{S/I} - T_{BS}\vec{\omega}_{B/I} \tag{A1}$$

Alternatively, it can be written using the Euler angle rates about the previously defined rotation axes as

$$\vec{\omega}_{S/B} = (-s_{\theta_S}\dot{\psi}_S)\vec{I}_S + (\dot{\theta}_S)\vec{J}_S + (c_{\theta_S}\dot{\psi}_S)\vec{K}_S \tag{A2}$$

Both expressions for angular velocity of the payload with respect to the parafoil must be equal. Equating (A1) and (A2) and expressing in compact matrix form results in

$$\begin{Bmatrix} p_S \\ q_S \\ r_S \end{Bmatrix} - T_{BS}\begin{Bmatrix} p_B \\ q_B \\ r_B \end{Bmatrix} = \begin{Bmatrix} -s_{\theta_S}\dot{\psi}_S \\ \dot{\theta}_S \\ c_{\theta_S}\dot{\psi}_S \end{Bmatrix} \tag{A3}$$

The parafoil and payload system is constrained so that there is no relative roll, only relative yaw ψ_s and pitch θ_s. However, because the system is a multibody three-dimensional problem, this does not imply that p_S is zero. Equation (A3) can rearrange so that the three unknowns (the two unknown Euler angle rates $\dot{\theta}_S$ and $\dot{\psi}_S$, and the constraint p_S) are isolated:

$$\begin{Bmatrix} 0 \\ q_S \\ r_S \end{Bmatrix} - T_{BS}\begin{Bmatrix} p_B \\ q_B \\ r_B \end{Bmatrix} = \begin{bmatrix} -1 & 0 & -s_{\theta_S} \\ 0 & 1 & 0 \\ 0 & 0 & c_{\theta_S} \end{bmatrix}\begin{Bmatrix} p_S \\ \dot{\theta}_S \\ \dot{\psi}_S \end{Bmatrix} \tag{A4}$$

Finally, the unknown constraint and Euler angle rates can be found using matrix inversion as

$$\begin{Bmatrix} p_S \\ \dot{\theta}_S \\ \dot{\psi}_S \end{Bmatrix} = \begin{bmatrix} 0 & -t_{\theta_S} \\ 1 & 0 \\ 0 & 1/c_{\theta_S} \end{bmatrix}\begin{Bmatrix} q_S \\ r_S \end{Bmatrix} + \begin{bmatrix} c_{\psi_S}/c_{\theta_S} & s_{\psi_S}/c_{\theta_S} & 0 \\ s_{\psi_S} & -c_{\psi_S} & 0 \\ -t_{\theta_S}c_{\psi_S} & -t_{\theta_S}s_{\psi_S} & -1 \end{bmatrix}\begin{Bmatrix} p_B \\ q_B \\ r_B \end{Bmatrix} \tag{A5}$$

References

[1] Carter, D., George, S., Hattis, P., McConley, M., Rasmussen, S., Singh, L., and Tavan, S., "Autonomous Large Parafoil Guidance, Navigation, and Control System Design," AIAA Paper 2007-2514, May 2007.

[2] Kaminer, I., and Yakimenko, O., "On the Development of GNC Algorithm for a High-Glide Payload Delivery System," *Proceedings of the IEEE Conference on Decision and Control*, Vol. 5, Inst. of Electrical and Electronics Engineers, New York, 2003, pp. 5438–5443.

[3] Slegers, N., and Costello, M., "Model Predictive Control of a Parafoil and Payload System," *Journal of Guidance, Control, and Dynamics*, Vol. 28, No. 4, 2005, pp. 816–821. doi:10.2514/1.12251

[4] Slegers, N., Kyle, J., and Costello, M., "A Nonlinear Model Predictive Control Technique for Unmanned for Air Vehicles," *Journal of Guidance, Control, and Dynamics*, Vol. 29, No. 5, 2006, pp. 1179–1188. doi:10.2514/1.21531

[5] Calise, A., and Preston, D., "Swarming/Flocking and Collision Avoidance for Mass Airdrop of Autonomous Guided Parafoils," *Journal of Guidance, Control, and Dynamics*, Vol. 31, No. 4, 2008, pp. 1123–1132. doi:10.2514/1.28586

[6] Slegers, N., and Yakimenko, O., "Optimal Control for Terminal Guidance of Autonomous Parafoils," *Proceedings of the 20th AIAA Aerodynamic Decelerator Systems Technology Conference and Seminar*, AIAA Paper 2009-2958, May 2009.

[7] Lissaman, P., and Brown, G., "Apparent Mass Effects on Parafoil Dynamics," AIAA Paper 93-1236, May 1993.

[8] Jann, T., "Aerodynamic Model Identification and GNC Design for the Parafoil-Load System ALEX," AIAA Paper 2001-2015, May 2001.
[9] Barrows, T., "Apparent Mass of Parafoils with Spanwise Camber," *Journal of Aircraft*, Vol. 39, No. 3, 2002, pp. 445–451. doi:10.2514/2.2949
[10] Slegers, N., Beyer, E., and Costello, M., "Use of Variable Incidence Angle for Glide Slope Control of Autonomous Parafoil," *Journal of Guidance, Control, and Dynamics*, Vol. 31, No. 3, 2008, pp. 585–596. doi:10.2514/1.32099
[11] Doherr, K., and Schilling, H., "Nine-Degree-of-Freedom Simulation of Rotating Parachute Systems," *Journal of Aircraft*, Vol. 29, No. 5, 1992, pp. 774–781. doi:10.2514/3.46245
[12] Slegers, N., and Costello, M., "Aspects of Control for a Parafoil and Payload System," *Journal of Guidance, Control, and Dynamics*, Vol. 26, No. 6, 2003, pp. 898–905. doi:10.2514/2.6933
[13] Mooij, E., Wijnands, Q., and Schat, B., "9 DOF Parafoil/Payload Simulator Development and Validation," AIAA Paper 2003-5459, Aug. 2003.
[14] Yakimenko, O., "On the Development of a Scalable 8-DOF Model of a Generic Parafoil-Based Delivery System," *Proceedings of the 18th AIAA Aerodynamic Decelerator Systems Technology Conference and Seminar*, AIAA Paper 2005-1665, May 2005.
[15] Müller, S., Wagner, O., and Sachs, G., "A High-Fidelity Nonlinear Multibody Simulation Model for Parafoil Systems," AIAA Paper 2003-2120, May 2003.
[16] Redelinghuys, R., "A Flight Simulation Algorithm for a Parafoil Suspending an Air Vehicle," *Journal of Guidance, Control, and Dynamics*, Vol. 30, No. 3, 2007, pp. 791–803. doi:10.2514/1.25074
[17] Strickert, G., and Jann, T., "Determination of the Relative Motion Between Parafoil Canopy and Load Using Advanced Video-Image Processing Techniques," AIAA Paper 99-1754, May 1999.
[18] Lamb, H., *Hydrodynamics*, Dover, New York, 1945, pp. 160–174.
[19] Mortaloni, P., Yakimenko, O., Dobrokhodov, V., and Howard, R., "On the Development of a Six-Degree-of-Freedom Model of a Low-Aspect-Ratio Parafoil Delivery System," *Proceedings of the 17th AIAA Aerodynamic Decelerator Systems Technology Conference and Seminar*, AIAA Paper 2003-2105, May 2003.